

Novel Aptamer-Functionalized Nanoparticles Enhances Bone Defect Repair By Improving Stem Cell Recruitment

This article was published in the following Dove Press journal:
International Journal of Nanomedicine

Meng Wang¹
Haibin Wu^{2,3}
Qiao Li⁴
Ying Yang²
Fengyu Che²
Guoxia Wang²
Liyu Zhang^{2,3}

¹Department of Orthopaedics, The NO. 946 Hospital of PLA, YiNing, Xinjiang 86-835000, People's Republic of China;

²Shaanxi Institute of Pediatric Diseases, Xi'an Children's Hospital, Xi'an, Shaanxi 86-710003, People's Republic of China;

³Key Laboratory of Environment and Genes Related to Diseases, Ministry of Education, Xi'an Jiaotong University Health Science Center, Xi'an, Shaanxi 86-710061, People's Republic of China;

⁴Clinical Laboratory, Xi'an Children's Hospital, Xi'an, Shaanxi 86-710003, People's Republic of China

Background: The restoration and repair method in the clinic of delayed fracture healing and non-union after comminuted fractures are urgently needed to improve the prognosis of patients. The recruitment of endogenous stem cells has been considered a promising approach in bone defect repair.

Propose: The aim of this study was to generate a de novel MSCs aptamer and developed the first, feasible, economical, bio-compatible, and functional MSCs aptamer-directed nanoparticles without complex manufacture to recruit mesenchymal stem cells (MSCs) for bone defect regeneration.

Methods: Whole-cell SELEX was used to generate a de novel MSCs aptamer. Flow cytometry was applied to assess the binding specificities, affinities and sorting abilities of the aptamers. Nano-Aptamer Ball (NAB) was constructed by NHS/EDC reaction. The diameter and zeta of NAB were assessed by dynamic light scattering. CCK8 assay was utilized to evaluate whether NAB could cause non-specific cytotoxicity and induce cell proliferation. To evaluate the bone repair capacity of NAB, histomorphological staining, alizarin red and micro X-ray were used to observe the repair degree of defect in vivo. ELISA was used to detect osteopontin (OPN), osteocalcin (BGP) by, and alkaline phosphatase (ALP) in peripheral blood.

Results: MSCs aptamer termed as HM69 could bind with MSCs with high specificity and Kd of 9.67 nM, while has minimal cross-reactivities to other negative cells. HM69 could capture MSCs with a purity of >89%. In vitro, NAB could bind and capture MSCs effectively, whereas did not cause obvious cytotoxicity. In vivo, serum OPN, BGP, and ALP levels in the NAB group of rats were increased at both 2 and 4 weeks, indicating the repair and osteogenesis generation. The healing of bone defects in the NAB group was significantly better than control groups, the defects became blurred, and local trabecular bone growth could be observed in X-ray. The organized hematoma and cell growth in the bone marrow of the NAB group were more vigorous in bone sections staining.

Conclusion: These suggested that HM69 and HM69-functionalized nanoparticles NAB exhibited the ability to recruit MSCs both in vitro and in vivo and achieved a better outcome of bone defect repair in a rat model. The findings demonstrate a promising strategy of using aptamer-functionalized bio-nanoparticles for the restoration of bone defects via aptamer-introduced homing of MSCs.

Keywords: comminuted fractures, bone defect, aptamer, mesenchymal stem cells, nanoparticles

Correspondence: Liyu Zhang
Shaanxi Institute of Pediatric Diseases,
Xi'an Children's Hospital, 69 West JuYuan
Alley, LianHu, Xi'an, Shaanxi 86-710003,
People's Republic of China
Tel +86 18066858662
Fax +86 02987692009
Email liyu_17@sina.com

Introduction

Comminuted fractures are common fractures in orthopedics, especially in high-energy injuries such as car accidents and high falling injuries. In addition to the numerous fracture fragments at the fracture end, comminuted fractures often

accompanied by severe surrounding tissue damage, even artery, vein and nerve damage, which are difficult to be restored.¹ Generally, surgical treatment methods such as intramedullary nail and lateral locking plate can repair and reset the fracture end.² Although when combined with autologous bone strut and cortico-cancellous bone grafting treatment, the surgical treatment made the prognosis acceptable in most cases,³⁻⁵ the delayed fracture healing and non-union after comminuted fractures are still a great challenge in clinical treatments. Retrospective studies have reported various nonunion rates following treatment with operation, ranging from 0% to as high as 20%,³ and these comminuted fracture patients often experienced delayed fracture healing and non-union and suffered from long-term pain, disability, and even osteomyelitis. Thus, the treatment of delayed fracture healing and non-union is essential for the patient outcome improvement.

Besides the common factors such as age, gender, smoking, drinking, obesity, and drugs that contribute delayed healing or even non-healing with bone defects,^{3,4} clinical and research findings have proven that two major factors affect the healing of bone defects mostly. Firstly, the compression or loss of the bone fragments leads to the defect of the fracture end. Secondly, the severe soft tissue damage caused by a fracture.⁵ It is all known that the soft tissue around the fracture end is especially important for the healing of the fracture,⁶ which is the guarantee of the early healing and the prevention of nonunion after surgery. Severe comminuted fracture may cause both fracture end defect and soft tissue damage, making it a terrible bone-soft tissue condition and objectively affecting the fracture healing process.^{7,8} At present, in order to prevent and improve the defect and nonunion after fracture, intraoperative bone grafting was often used to patch the bone defect during the surgery.⁹ The patient's autologous bone (usually taken from ilium and fibula) or artificial bones were implanted to the bone defect to promote fracture healing. In addition, to repair the soft tissue injury problem in comminuted fractures, standard and skilled operation must be guaranteed to minimize the damage to the periosteum, peripheral muscles and other soft tissues, and the damaged blood vessels and nerves should be repaired as well, which is no reliable treatment in clinical work. The current clinical surgical treatments have little effects on the bone defects caused by a comminuted fracture. Therefore, to date, the bone defects caused by comminuted fracture are difficult to restore, none of the clinical treatments are able to fully restore injured bone defects after

comminuted fractures. Therefore, the restore and repair method in the clinic of bone defects is urgently needed and to improve the prognosis of patients.

Mesenchymal stem cells (MSCs), kind of bone marrow-derived cells, are capable of differentiating into multiple cell types because of their self-renewing ability and multipotent progenitors.¹⁰ At present, MSCs have been most widely used in biological tissue repair and engineering, such as in respiratory system disease,¹¹ nervous system disease,¹² endocrine system disease,^{13,14} cardiovascular system disease,¹⁵ etc. Therefore, utilizes MSCs from the bone marrow to migrate toward the injury site and stimulate into chondrocytes to repair bone defect, is a promising choice for comminuted fracture repair.^{16,17} Exogenous MSCs transplantation is one way for MSCs transplantation. However, the long-term clinical outcome may be usually less than satisfactory: Exogenous MSCs tend to undergo hypertrophic differentiation, which finally results in calcification. Since MSCs are abundant in other joint tissues such as subchondral bone, synovial fluid, synovium, and adipose tissue, bone defect repair by recruiting endogenous stem cells in situ has been given much attention.¹⁸ However, the number of the MSCs spontaneously migrating toward the bone defect might be insufficient to regenerate cartilage of such volume, there is a major need to develop a novel targeted molecule which could collect endogenous MSCs selectively in vivo.

Aptamers, which are called as "synthesized antibody", are a kind of novel targeted molecules with potential clinical application.¹⁹ Aptamers are short, single-stranded oligonucleotides (DNA or RNA), and can bind to their targets with high affinity and specificity by folding into tertiary structures.²⁰ When compared with typical targeted molecules antibodies, aptamers have a number of advantages, such as high affinity for binding to target molecules, limited synthesis cost, no batch-to-batch variability, higher target potential ranging from ions to live cells, small sizes that allows them to penetrate tissues and non-immunogenic, which may facilitate long-term therapeutic efficacy and safety.²¹ Most noteworthy is that on account of geometrical conformational flexibility and synthesis dynamics, aptamers can be readily synthesized and chemically modified for various therapeutic applications.²² Thus, since the first RNA aptamer developed in 1992,²³ aptamers have been extensively developed and used in clinical diagnostics, therapeutic agents and tissue engineering applications. There have several works of literature reported that aptamer can capture and enrich targeting cells with relatively high

efficiency and accuracy, and aptamer has been widely used in the capture of circulating tumor cells (CTCs).^{24–26} Thus, an aptamer-directed repair system capable of selective recruitment of MSCs to the comminuted fracture defect site would open a new promising path for bone defect repair. So far, however, the research on the employment of MSC aptamer for capture, recruitment of MSCs and further repairment for tissue engineering application of comminuted fracture has not been reported.

Here in this study, we tried our first attempt to develop a novel MSCs aptamer by Cell-SELEX technique and constructed functional aptamer-based nanoparticles to recruit endogenous stem cells to bone defect for repair and restore. We have successfully selected a 66-based DNA aptamer (termed HM69) against MSCs. We evaluated the binding specificity and affinity of HM69 and found that HM69 could recognize and bind with MSCs with high specificity and affinity. Furthermore, HM69 could capture MSCs *in vitro*. In addition, nanoparticles constructed from HM69, termed as NAB, could capture and enrich MSCs to bone defect *in vivo*, resulting in excellent performance for bone defect repair and restore. Overall, these results proved that novel MSCs aptamer HM69 is a useful tool for MSCs recognition, capture and enrichment, and HM69-based nanoparticle NAB is a novel potential approach for bone defect repair and restore of comminuted fracture in the clinic.

Materials And Methods

Reagents

ssDNA library for SELEX and primers were synthesized by Sangon Biotech (Shanghai China), bovine serum albumin (BSA, Sigma-Aldrich, Japan, Catalogue#:V900 933), DMEM/F12 medium (Gibco, US, Catalogue#: 12400-024), Fetal bovine serum (Gibco, US, Catalogue#: 16000-044), trypsin (Sigma-Aldrich, Japan, Catalogue#: T2600000), cell counting kit 8 (CCK8, Sigma-Aldrich, US, Catalogue#:96992), Rat osteopontin (OPN) ELISA kit (Cusabio, Wuhan, China, Catalogue#: CSB-E08392h), osteocalcin (BGP) ELISA kit (Sigma-Aldrich Co. LLC., Shanghai, China), Alkaline phosphatase (ALP) (Sigma-Aldrich Co. LLC), streptavidin-coated magnetic beads (Promega, Madison, WI), 1-ethyl-3-(3-dimethylaminopropyl)-carbodii-mide hydrochloride (EDC, Sangon Biotech, Shanghai, China, Catalogue#:C600433), N-Hydroxysuccinimide (NHS, Sangon Biotech, Shanghai, China, Catalogue#:C100219).

Cell Lines

The human ESC cell line, mouse embryonic stem cell line (mES), rhesus ES cells, 293FT cell line, BJAB cell line (Human B-cell lymphoma), trophoblast cells, human cardiac fibroblast HCFB and PA317 mouse fibroblast cells were obtained from ATCC (American Type Culture Collection). The Molm-13 human acute myelocytic leukemia, K562 human myeloid leukemia cells, RCH-ACV human B-cell precursor leukemia cell lines and Ramos human B lymphoma cell lines were obtained from Cell Culture Centre of Peking Union Medical College (Beijing, China) in 2016. Human ESC cells were cultured in E8 medium on Matrigel-coated plates. mES, rhesus ES cells, 293FT cell line, BJAB cell line, and trophoblast cells were cultured in DMEM/F12 medium, Molm-13, K562, RCH-ACV and Ramos cells were cultured in 1640 medium, HCFB and PA317 cells were cultured in DMEM medium. All cells were supplemented both with 10% fetal bovine serum (Sigma) at 37°C in humidified air containing 5% CO₂ and maintained by routine passage every 2–3 days. All experiments were performed on cells in the exponential growth phase.

Whole-Cell SELEX

The DNA library contained a central randomized sequence of 28 nucleotides flanked by two 19 nucleotides PCR primer hybridization sites (5'-TGCGTGTGTAGTGTGTCTG-(N28)-CTCTTAGGGATTGGGCGG-3'), FITC/FAM-labeled forward primer (5'-TGCGTGTGTAGTGTGTCTG-3') and biotin-labeled reverse primer (5'-CCGCCCAAATCCCTAAGAG-3'). Human ESC cells were used as the target cell line and 293FT as the control cell line. To furthest improve selection efficacy and reduce selection non-specificity, we did the pre-SELEX procedure before typical SELEX. BSA (1 mg) was coated on plates in advance. The single-stranded DNA (ssDNA) library (1 nmol) in 1000 μL was heated up to 95°C for 5 mins and cooled on ice immediately. These ssDNA were added in the BSA-coated plate for 30 mins to maximally exclude nonspecific sequences. SELEX procedure was as follows: The treated DNA library was incubated with human ESC cells (2.5×10⁶ cells) for 45 mins at 37°C. To reduce background, 0.1 mg/mL salmon sperm DNA and 1 mg/mL of BSA were added to the binding buffer. The unbound oligonucleotides were removed by washing Cells with PBS buffer twice. Subsequently, PBS was added into cells and heated at 95°C, the supernatant was collected. Then, a counter-selection was performed by incubating supernatant with 293FT cells

(5×10^6 cells) for 45 mins at 37°C. The supernatant was amplified by PCR with FITC- or biotin-labeled primers (25 cycles of 30 s at 95°C, 30 s at 56°C, 30 s at 72°C, followed by 10 mins at 72°C). Lastly, dsDNA from PCR was separated into ssDNA via the procedure described earlier. The FITC-ssDNA was used for the next round of SELEX. After 9 rounds, the DNA was sequenced by the next-generation sequencing (NGS). The 9th PCR product was then run on HiSeq2000 (Illumina) with a Single Read 80 Base Pair program to obtain the whole aptamer sequence and the index. We transformed the aptamers to sense strand based on matching the primer regions. The sequences were analyzed, and the highest abundance sequence was chemically synthesized for further research.

Aptamer-Binding Characteristics Assays

To evaluate the binding characteristics of aptamer, binding specificity and binding affinities were assessed. Firstly, to assess the binding specificity of aptamer, the FAM-labeled aptamer (60 pM) was separately incubated with 1×10^5 MSCs or 293FT cells at 37 °C for 30 mins. Cells were washed by PBS (500 μ L) twice and analyzed by flow cytometry (BD FACS Calibur, NJ).

To evaluate the binding affinity of the aptamer to MSCs, gradient concentrations of FAM-labeled aptamer were incubated with 1×10^5 H1 cells at 37°C for 30 mins. Cells were washed three times and resuspended in 0.2 mL PBS buffer and subjected to flow cytometric analysis. 293FT cells were treated as negative controls to measure nonspecific binding. All of the experiments for binding assay were repeated three times. The mean fluorescence intensity of target labeled by aptamers was used to calculate for specific binding by subtracting the mean fluorescence intensity of nonspecific binding to 293FT cells. The equilibrium dissociation constants (Kd) of the aptamer-MSCs were obtained by fitting the dependence of fluorescence intensity of specific binding on the concentration of the aptamers to the equation: $Y = B_{\max} X / (Kd + X)$ ²⁷

Selective Binding Study Of HM69

To assess whether HM69 could recognize and bind with MSCs cells selectively, FITC-labeled HM69 (10 mM) was incubated with either 1×10^5 MSCs, BJAB cell line, trophoblast cells, K562, Molm-13, Hela, Ramos, MCF-7, RCH-ACV, HCFB or PA317 cells at 37°C for 30 mins. Cells were washed three times and resuspended by PBS. Then, the cells were analyzed by flow cytometry.

Sorting Ability Assessment Of Aptamers

To assess whether aptamer could sort MSCs selectively, cells sorting assay were performed. Firstly, 1×10^5 MSCs were labeled by carboxyfluorescein diacetate succinimidyl ester (CFSE). In brief, CFSE dye was diluted by PBS (5 mM). MSCs were incubated with CFSE and kept in darkness for 10 mins. Cells were centrifuged and washed by PBS twice. Secondly, these labeled cells were mixed with 3×10^5 unlabeled 293FT cells. Aptamer was labeled by biotin and fixed on the streptavidin-coated magnetic beads. Subsequently, the mixed cells were incubated with beads at 37°C for 30 mins. Beads were collected in the magnetic field and the supernatant was analyzed by flow cytometry and observed by a fluorescence microscope. Mixed cells incubated with random DNA-coated beads were treated as a control group. Further, to determine the sorting specificity of HM69 with a more complex cell mixture, a selective sorting study with blood cells in a co-culture setting was utilized. Firstly, MSCs were labeled with CFSE as described above. Then, rat peripheral blood was centrifuged, and the cells were mixed with labeled MSCs. HM69 was labeled by biotin and fixed on the streptavidin-coated magnetic beads. The mixed cells were incubated with beads at 37°C for 30 mins. Beads were collected in the magnetic field and the supernatant was analyzed by flow cytometry.

Construction And Assessment Of Nano-Aptamer Ball (NAB)

To construct a poly-aptamer, the aptamer was labeled $-NH_2$ at 3' and $-COOH$ at 5' end. Fifty mM aptamer was dissolved in 200 μ L MES (100 mM, pH 5.0) at room temperature. Then, aptamer was activated by 100 μ L 1-ethyl-3-(3-dimethylaminopropyl)-carbodiimide hydrochloride (EDC) (20 mg/mL) for 15 mins with gentle stirring, and 100 μ L N-hydroxysuccinimide (NHS) (20 mg/mL) was added to generate the chemical bonding between $-NH_2$ and $-COOH$. The mixture was incubated at room temperature for further time (0.5 hr, 1 hr, 1.5 hrs, 2 hrs, 3 hrs, 4 hrs, and 6 hrs). Subsequently, the mixture was centrifuged at 12,000 rpm for 10 mins and the sediment at the bottom was collected and washed by PBS twice. To evaluate the diameter and zeta of NAB, NAB was diluted in PBS and the diameter was assessed by Dynamic Light Scattering (DLS).

In Vitro Cytotoxicity Assay

To evaluate whether NAB could cause non-specific cytotoxicity to cells, cell viability was detected by CCK8 assay.

Human ES cells, mES, rhesus ES cells, 293FT cell line, BJAB, and trophoblast cells were seeded in 96-well plates and treated with NAB or random DNA at various concentrations (10 nM, 20 nM, 40 nM, 60 nM, 80 nM, 100 nM, 120 nM, 150 nM, 300 nM, 400 nM, 600 nM) at 37°C. After 24 hrs, cells were washed with PBS buffer and CCK8 assay was used to determine the cell viability per standard protocol outlined by the manufacturer's instruction.

In Vitro Cell Proliferation Assay

To evaluate whether NAB could induce cell proliferation, 1×10^5 cells (mES, rhesus ES cells, and human ES cells) were incubated at 96-well plate and simultaneously with 120 nM random DNA or NAB. Then, cells were washed and further incubated for different times. Cell culture supernatant fluids were collected at 0, 6, 12, 24, 36 and 48 hrs, and were analyzed with a CCK-8 kit to determine the cell viability.

MSCs Enrichment Capacity Assessment Of NAB

To evaluate whether NAB could enrich MSCs selectively, 1×10^3 MSCs were seeded in the 6-well plates. NAB or random DNA was added into the plate and incubated for 30 mins. Then, PBS was used to wash cells twice, and another 1×10^3 MSCs were added and incubated for 30 mins. Next, PBS was used to wash un-bonded cells. Cell culture was added, and cells were cultured for another 24 hrs. Cells were stained by crystal violet and observed by a microscope. Cell number was assessed to evaluate whether NAB had enriched MSCs. Further, to determine the sorting specificity of NAB with a more complex cell mixture, a selective sorting study with blood cells in a co-culture setting was utilized. Firstly, MSCs were labeled with CFSE as described above. Then, rat peripheral blood was centrifuged, and the cells were mixed with labeled MSCs. NAB was labeled by biotin and fixed on the streptavidin-coated magnetic beads. The mixed cells were incubated with beads at 37°C for 30 mins. Beads were collected in the magnetic field and the supernatant was analyzed by flow cytometry.

Evaluation Of Bone Defects Reconstruction Ability Of NAB In Vivo

The ethical and legal approval of animal study in this paper was obtained prior to the commencement of the study by the ethics Committee of Xi'an Children's Hospital, Xi'an, China (no. C2018004). All animal experiments were

conducted in accordance with institutional regulations. All experiments were performed following relevant named institutional and national guidelines and regulations. Six-week-old male Sprague Dawley rats were purchased from the Xi'an JiaoTong University Lab Animal Centre (Xi'an) and raised under pathogen-free conditions. To evaluate the bone repair capacity of NAB, a full-thickness penetrating defect was created in the lower and middle third region of each rat femur. Rats were randomly divided into three groups, with six in each group: i) treated with NAB (2 mg/kg); ii) treated with random DNA library (2 mg/kg); and iii) treated with saline. Drugs were administered through regional injection once 2 days. Subsequently, 2 rats from each group were euthanized at 0, 2 and 4 weeks after drilling. Rat peripheral blood in each group was collected to detect osteopontin (OPN), osteocalcin (BGP) by ELISA, and alkaline phosphatase (ALP) was measured using p-Nitro phenyl phosphate colorimetric determination. All tests were performed per manufacturers' instructions. The femurs were collected. Sections of the femur samples were applied for histomorphological staining. Half of the sections from each group were stained by H&E after EDTA decalcification to evaluate the hematoma reactions of bone marrow. The other sections were stained by alizarin red to observe the calcium content, which indicated the activity of osteoblasts. Micro X-ray was used to observe the repair degree of defect.

Statistics

All numerical data were expressed as the mean \pm S.D. Statistical differences between two groups were determined by the Student's *t*-test. $p < 0.05$ was considered statistically significant.

Results

Hypothesis Of NAB For Comminuted Fracture Repair

The NAB platform is poly-MSCs-aptamer-originated nanoparticles, which is assembled by -NH-CO- chemical cross-linking between MSCs aptamers. In detail, as shown in [Figure 1A](#), each MSCs aptamer are both labeled with -NH₂ at 3' end and -COOH chemical group at 5' end. The -NH₂ of one aptamer could interact with -COOH of another aptamer forming -NH-CO- under NHS and EDC condition. Thus, MSCs aptamers are linked one by one and will fold into nanoball under aqueous solution which termed as NAB. After NAB injection into bone, as presented in

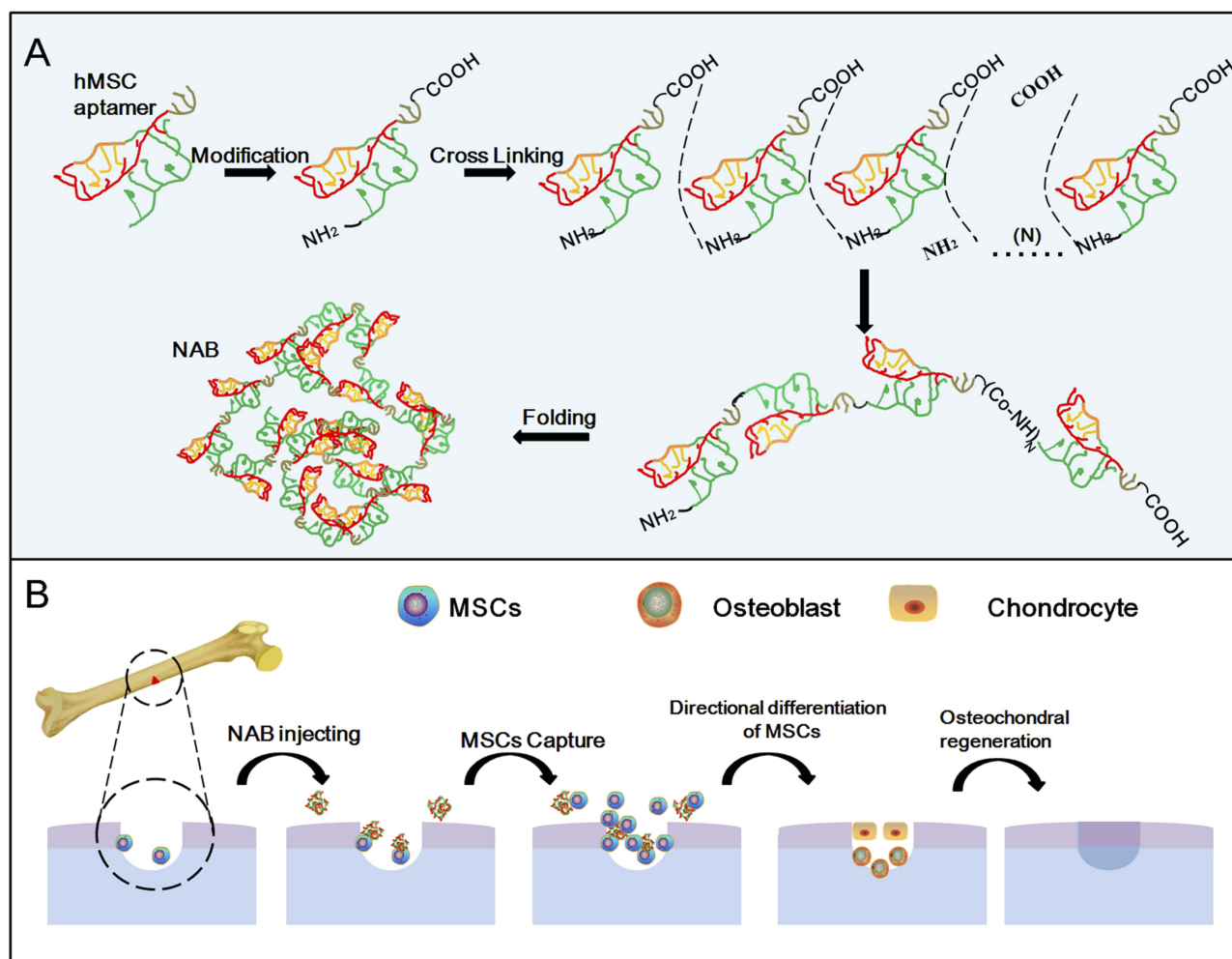


Figure 1 Study design and experimental scheme of aptamer-functionalized nanoparticles for targeting MSCs recruitment for bone defect restoration in theranostic applications. **(A)** Preparation of NAB based on aptamer HM69. Aptamer HM69 was modified -NH_2 at the 3' end and -COOH at the 5' end, respectively. Modified HM69 was linked with each other under NHS/EDC system and generate -NH-CO- chemical bond. Then, poly-HM69 tended to be a nanoparticle in an aqueous solution. **(B)** Schematic diagram of bone defect. After the NAB injection, NAB could firstly recognize the MSCs in bone defect and be anchored. Secondly, NAB could capture and recruit MSCs to bone defect. Then, more MSCs may differentiate into chondrocyte and osteoblast.

Abbreviations: EDC, 1-ethyl-3-[3-dimethylaminopropyl] carbodiimide hydrochloride; NHS, N-hydroxysuccinimide.

Figure 1B, when a bone defect was generated, there were little MSCs nearby which was not sufficient to repair. When NAB was injected, NAB could firstly recognize and bind to MSCs with high specificity and affinity, and be anchored in bone defect. Therefore, since NAB could capture more MSCs, more and more MSCs in blood and other joint tissues could be captured by NAB and enriched in bone defect. Thus, more MSCs will differentiate into osteoblast and chondrocyte to repair the bone defect.

Whole Cell-SELEX And Monitoring Of Aptamer Selection Process

The target of SELEX process was whole MSC cells. SELEX procedure is shown in Figure 2. In detail, the random ssDNA

pool employed contained 66-mer oligonucleotides. When folding into three-dimensional structure, this high complexity ssDNA library could generate at least 10^{15} species of sequences. Generally, this diversity could fulfill SELEX procedure completely. Since albumin is the most abundant protein in the blood, to improve SELEX efficiency and effectiveness, an initial random ssDNA pool was firstly incubated with BSA to remove clones that bind with BSA. Then, the DNA pool was turned into the cell-SELEX procedure. hES cells were applied as positive cells and 293FT were treated as negative cells. SELEX procedure contains positive and negative screening. To monitor the efficacy of Cell-SELEX, the enriched aptamers were labeled by FITC and incubated with cells. The mean fluorescence intensities were assessed by flow cytometry. As presented in Figure 3, when

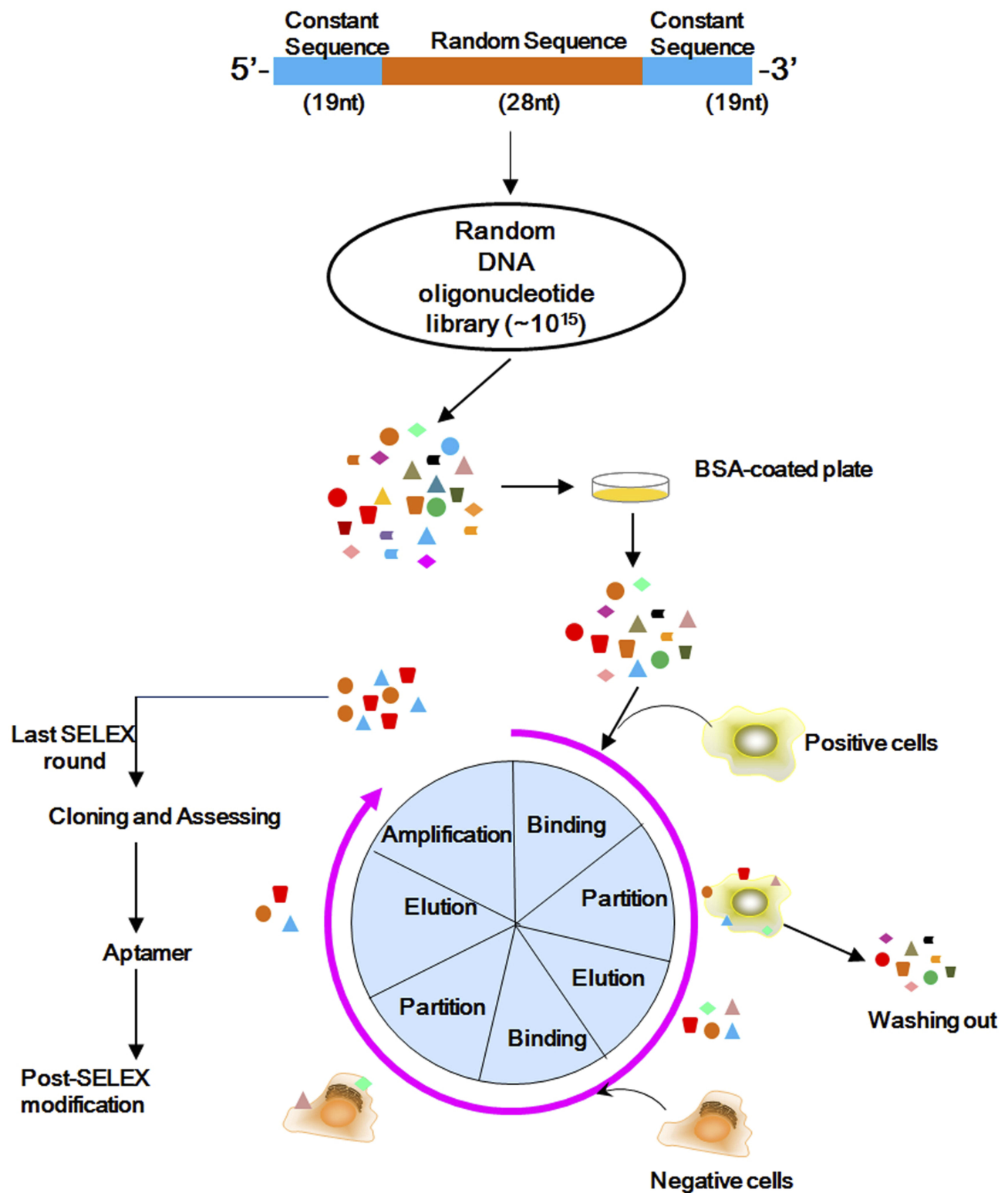


Figure 2 Scheme of whole cell-based SELEX process. Briefly, random DNA sequences contain 66-mer oligonucleotides with 28-base long randomized in central and fixed sequences at both sides. When folded into a three-dimensional structure, it became a high complexity ssDNA library that could satisfy SELEX completely. Random DNA library was firstly incubated with BSA to remove non-specific clones. The process of SELEX involves several steps: firstly, the nucleic acid library is incubated with a target (positive selection), which can be preceded or followed by a counter-selection phase to remove non-specific nucleic acid molecules. During the partitioning step, bound and unbound DNAs are separated. The bound fraction is amplified to obtain an enriched pool for the next round of selection. This process is repeated for N rounds until the pool is enriched for sequences that specifically bind the target. These nucleic acid molecules are cloned and sequenced.

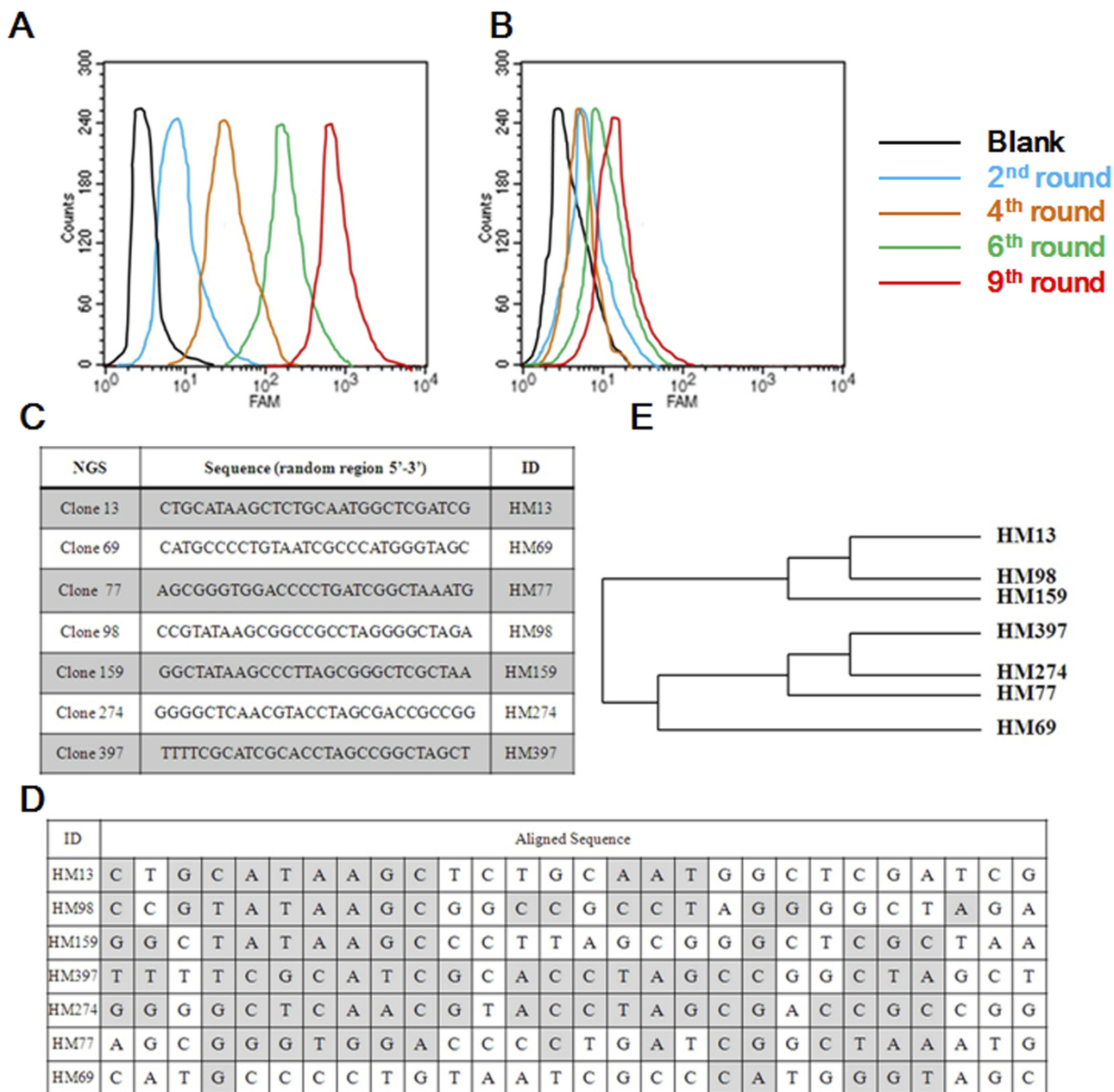


Figure 3 Monitoring of SELEX and DNA sequence analysis. (A) Flow cytometry monitoring of the enrichment of aptamers. Compared with the starting random DNA pool (the black curve), flow cytometry revealed an increase in fluorescence intensity of aptamers bound to the MSCs after the second (the blue curve), the fourth (the orange curve), the sixth (the green curve), and ninth (the red curve) rounds of selection. (B) Flow cytometry monitoring of the non-specific binding to 293FT of aptamers. (C) The random sequence of aptamers which were capable of binding MSCs preferentially. (D) The sequence alignment of aptamer candidates. (E) The similarity among the aptamer candidates was analyzed through the homology tree.

compared with the negative 293FT cell group (Figure 3B), there is an increasing amount of ssDNA bound to MSCs after each round of selection (Figure 3A). The ssDNA targeting to positive cells was furthest enriched at the 9th selection round and the DNA pool was sequenced by the next-generation sequencing (NGS) to be identified. As a result of NGS analysis, 7 sequences showing the highest abundance among approximately 0.8×10^4 raw sequences of data

(Figure 3C). The similarity among the aptamer candidates was analyzed through the homology tree (Figure 3D) and sequence alignment (Figure 3E).

Evaluation Of Aptamers' Binding Specificity And Affinity

To evaluate whether these 7 selected sequences could selectively recognize MSCs, binding specificity assay was

performed. MSC cells were utilized as positive cells, 293FT cells were treated as negative cells. Specifically, FITC-labeled clones and random DNA library were incubated with cells and the fluorescence intensities were evaluated by flow cytometry. As shown in [Figure 4A](#), all these seven clones exhibited relatively strong binding to MSCs, but a relatively weak binding to 293FT. These data indicated that all these clones could recognize MSCs with high specificity. Further, to assess these aptamers' structures, their secondary structures were predicted by M-fold website. As shown in [Figure 4B](#), all these DNA clones showed unique stem ring structures. We speculated that these special structures were the basis for their MSCs binding specificities. Binding affinity is another important parameter to evaluate aptamers. Since clone 69, 77 and 397 showed a relatively better specificity than other clones, we further assessed their binding affinities. To quantitatively assess the binding affinity, specifically, various concentrations FITC-labeled clone 69, 77 and 397 were incubated with MSCs. Random DNA library was treated as a negative control. After calculating by nonlinear regression analysis, the binding Kd of clone 69 was 9.67 nM, of clone 77 was 30.89 nM and of clone 397 was 58.13 nM ([Figure 4C](#)). Since clone 69 exhibits better performance of binding specificity and affinity, it was termed as HM69 and applied for further investigations.

Aptamer HM69 Recognized And Bound With MSCs With High Specificity

Furthermore, to evaluate whether HM69 retained its binding specificity to MSCs with high specificity, to address this question, binding specificity tests were performed. FITC-labeled HM69 was incubated with either positive cells (MSCs) or negative cells (BJAB cell line, trophoblast cells, K562, Molm-13, HeLa, Ramos, MCF-7, RCH-ACV, HCFB or PA317 cells) under the same experimental conditions and the cells were analyzed by flow cytometry. FITC-labeled random DNA was used as a background control. As presented in [Supplementary Figure 1](#), HM69 exhibited strong binding to MSCs, whereas binding to other eleven kinds of negative cells was quite weak. Furthermore, random DNA exhibited no binding preference to any of the cell lines. These results indicated that HM69 preferentially recognizes and binds with MSC cells in vitro.

Aptamer HM69 Enriched MSCs Effectively In Vitro

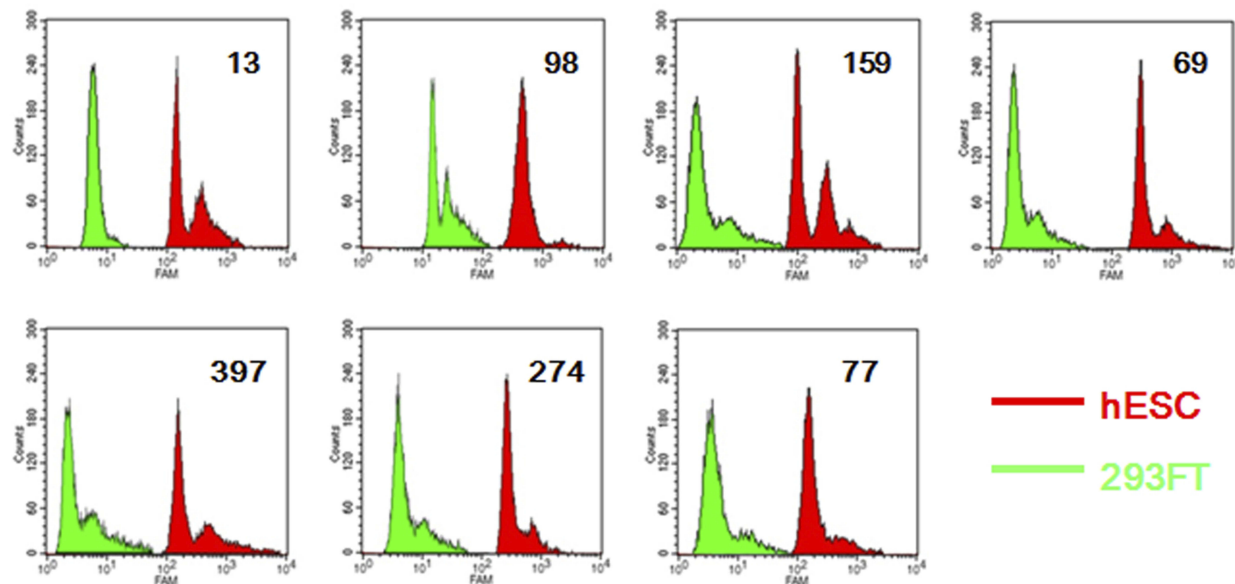
To evaluate whether HM69 could enrich MSCs, firstly, biotin-labeled HM69 was fixed on streptavidin-labeled

magnetic beads. Random DNA library was treated as a control group. Secondly, MSCs were stained by CFSE and mixed with unlabeled human 293FT cells. Cell mixture was measured by flow cytometry. Then, HM69-coated magnetic beads were incubated with cell mixture for 30 min. Beads were collected in the magnetic field and analyzed by flow cytometry. The supernatant was analyzed by flow cytometry and observed by a fluorescence microscope. As shown in [Figure 5A](#), after a single purification with HM69, the CFSE fluorescence of supernatant in the HM69 group decreased significantly when compared with random DNA group. We obtained MSCs with a purity of >89% after a single purification with HM69 from a cell mixture containing only ~25% of MSCs. However, the fluorescence in random DNA library group did not change significantly ([Figure 5B](#)). Further, supernatant was observed by a fluorescence microscope. As presented in [Figure 5C](#), MSCs were significantly reduced in HM69 group when compared with random DNA library group, indicating a successful capture of MSCs by HM69-coated beads. To further determine the sorting specificity of HM69 with more complex cell mixture, selective sorting study with blood cells in co-culture setting was utilized. CFSE labeled MSCs were mixed with rat peripheral cells and incubated with HM69-beads at 37°C for 30 mins. Beads were collected in magnetic field and the supernatant was analyzed by flow cytometry. As shown in [Figure 5D](#), after a single purification with HM69, the CFSE fluorescence of supernatant in HM69 group decreased significantly when compared with random DNA group. However, the fluorescence in random DNA library group did not change significantly ([Figure 5D](#)). These data indicated that HM69 could enrich MSCs with high specificity and efficiency.

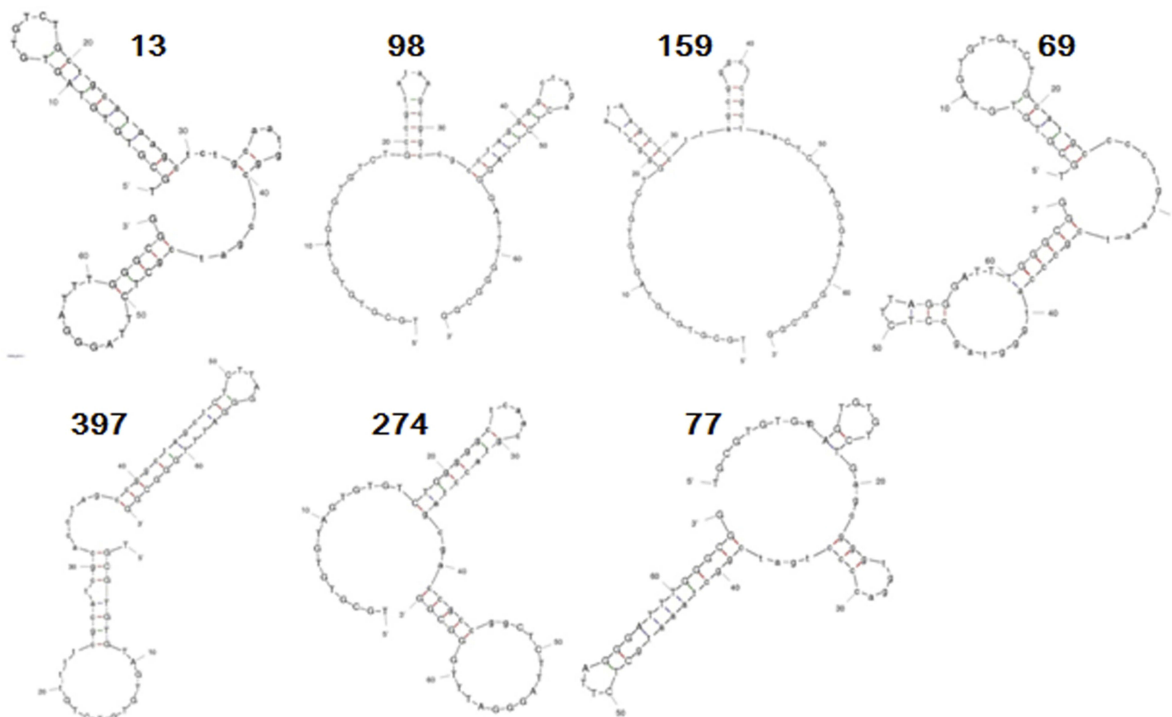
Construction And Characterization Of NAB

According to the hypothesis, to construct NAB, aptamer HM69 was chemically modified by $-NH_2$ at 3' end and $-COOH$ at 5' end. NAB was constructed by a chemical bond between $-NH_2$ and $-COOH$ under EDC/NHS condition. To control the diameter of NAB, the time of chemical bonding creation between $-NH_2$ and $-COOH$ was controlled for 0.5 hr, 1 hr, 1.5 hrs, 2 hrs, 3 hrs, 4 hrs, and 6 hrs. The products were assessed by DLS. As shown in [Figure 6A](#) and [B](#), the diameter of NAB ([Figure 6A](#)) increased and zeta potential ([Figure 6B](#)) decreased

A



B



C

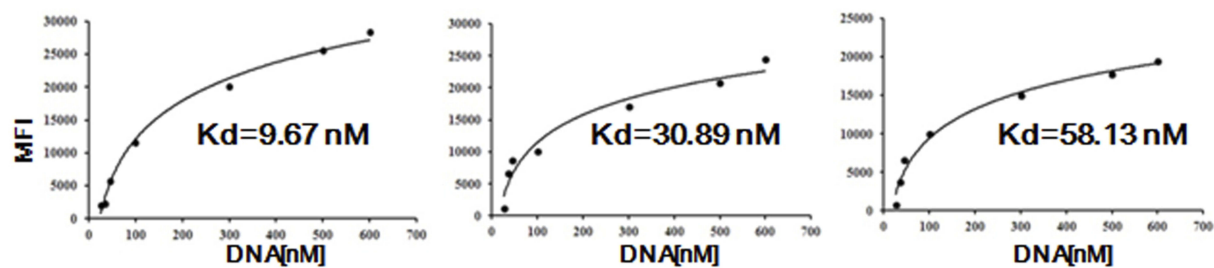


Figure 4 Characterization of aptamers candidates. (A) Evaluation of aptamers candidates' binding specificities. Flow cytometry evaluation of the binding specificity to MSCs (the red curve) or negative 293FT cells (the green curve) by FITC-labeled aptamer candidates (clone 13, 98, 159, 69, 397, 274, and 77). (B) The predicted secondary structure of aptamer candidates. The secondary structures of aptamer candidates were predicted by M-fold software. (C) Flow cytometry evaluation of the binding affinities to MSCs by FITC-labeled aptamers 69, 77, and 397.

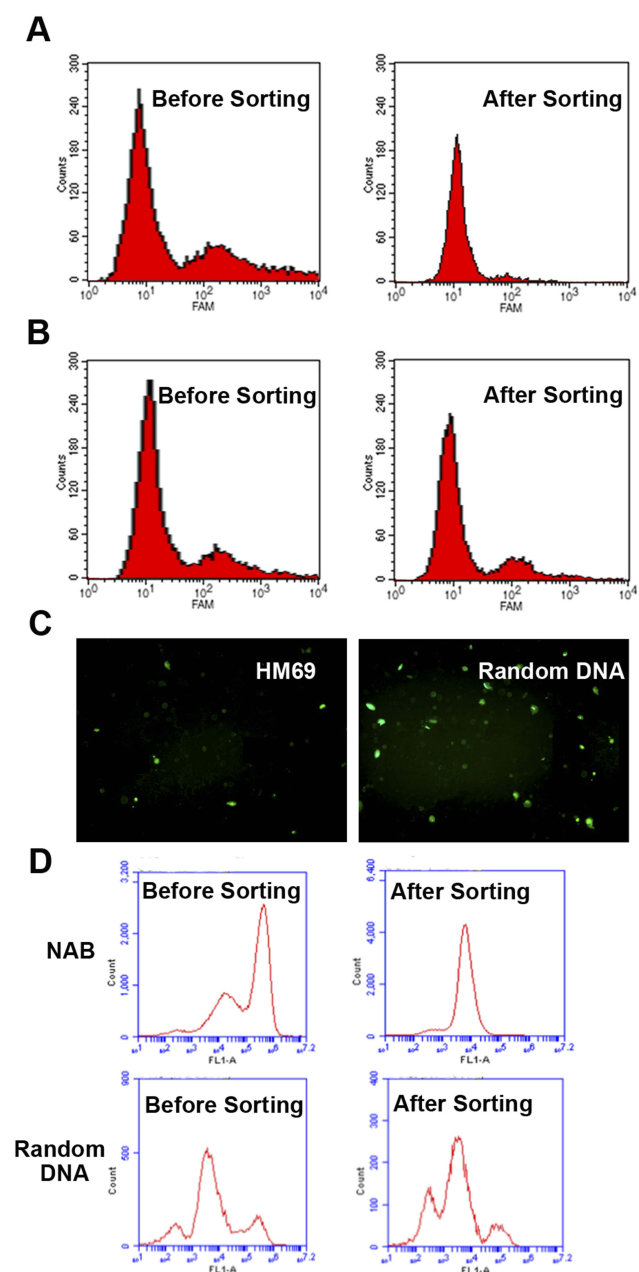


Figure 5 The MSCs sorting ability assessment of aptamer HM69. (A–C) The MSCs sorting ability assessment of aptamer HM69 with two cell lines: HM69 or random DNA was fixed on magnetic beads and incubated with a mixture of CFSE labelled MSCs and 293FT. After incubation, magnetic beads were collected under a magnetic field. The supernatant was analyzed by flow cytometry. (A) Flow cytometry of supernatant in HM69 group; (B) Flow cytometry of supernatant in random DNA group; (C) The fluorescence microscope images of two groups. (D) Flow cytometry of MSCs sorting ability assessment of aptamer HM69 with mouse peripheral blood: HM69 or random DNA was fixed on magnetic beads and incubated with a mixture of CFSE labelled MSCs and mouse peripheral blood. After incubation, magnetic beads were collected under a magnetic field. The supernatant was analyzed by flow cytometry.

significantly within the first 3 hrs, indicating the rapid synthesis of NAB. When incubation time was over 4 hrs, the diameter and zeta potential of NAB were quite stable, indicating the ending of synthesis. This may be caused by

the depletion of synthetic material. These results indicated that synthesis of NAB via EDC/NHS was feasible.

Further, to evaluate whether NAB could cause cytotoxicities to cells, mES, rhesus ES cells, hES cells, 293FT cell line, BJAB, and trophoblast cells were treated with NAB or random DNA at various concentration and cell viabilities were assessed by CCK8 assay. As shown in Figure 6C, when compared with random DNA group, NAB group showed no significant difference, indicating NAB did not cause obvious cytotoxicity.

NAB Could Capture And Enrich MSCs Effectively

To evaluate whether NAB could capture and enrichment MSCs, to assess whether NAB could induce cell proliferation of MSCs, mES, rhesus ES cells, and human ES cells were incubated with random DNA or NAB and cell viabilities were determined with a CCK-8 kit at 0, 6, 12, 24, 36 and 48hrs. As shown in Supplementary Figure 2, cell viabilities of three cell lines increased both in NAB and random DNA group, and there was no obvious significant difference between two groups ($P > 0.05$). These results indicated that NAB could not induce cell proliferation itself. Further, MSCs were seeded in 6-well plates and incubated with NAB for 30 mins. Then, PBS was used to wash cells twice, and another 1×10^3 MSCs were added and incubated for 30 mins. Next, PBS was used to remove un-bonded cells. Cells in 6-well plates were cultured for further 24 hrs. Cell number was assessed by crystal violet staining and observed under a microscope. As shown in Figure 6D, when compared with random DNA library group, cell number in NAB group increased significantly, whereas cell number did not change in random DNA library group. In addition, since NAB was designed to apply in vivo, whether it could maintain its sorting ability within blood cells should be assessed. Therefore, to further determine the sorting specificity of NAB with more complex cell mixture, selective sorting study with blood cells in co-culture setting was utilized. MSCs were labeled with CFSE and mixed with rat peripheral blood cells. NAB was fixed on the streptavidin-coated magnetic beads and incubated with cell mixture at 37°C for 30 mins. Beads were collected in the magnetic field and the supernatant was analyzed by flow cytometry. As shown in Supplementary Figure 3, after a single purification with NAB, the CFSE fluorescence of supernatant in NAB group decreased significantly when compared with random DNA group. However, the

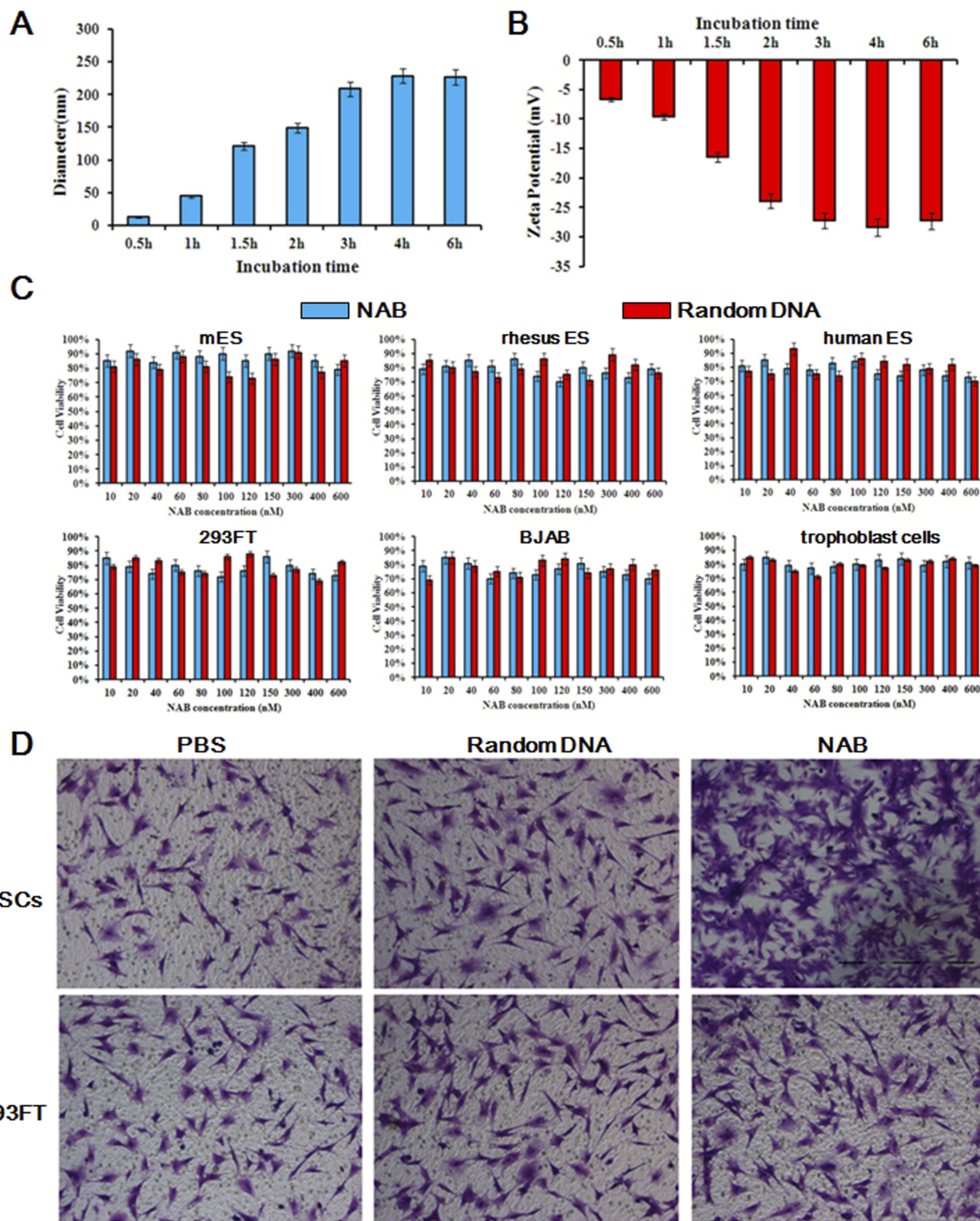


Figure 6 Construction and characterization of NAB. Aptamer HM69 was chemically modified by $-NH_2$ at 3' end and $-COOH$ at 5' end. NAB was constructed by a chemical bond between $-NH_2$ and $-COOH$ under EDC/NHS condition. To control the diameter of NAB, the time of chemical bonding creation between $-NH_2$ and $-COOH$ was controlled for 0.5 hr, 1 hr, 1.5 hrs, 2 hrs, 3 hrs, 4 hrs, and 6 hrs. The products were assessed by DLS. **(A)** The diameter of NAB. **(B)** The zeta potential of NAB. **(C)** Cytotoxicity Evaluation of NAB. Various concentrations of NAB were incubated with several cell lines and cell viabilities were assessed by CCK8 assay. Random DNAs were treated as control. **(D)** MSCs capture and enrich ability assessments of NAB. MSCs and 293FT were seeded in 6-well plates and incubated with NAB. Un-bonded DNAs were washed by PBS and another 1×10^3 MSCs were added and incubated for 30 min. PBS was used to remove un-bonded cells. Cells in 6-well plates were cultured for further 24 h. Cell number was assessed by crystal violet staining and observed under a microscope. Random DNAs were treated as control group.

fluorescence in random DNA library group did not change significantly. These data indicated that NAB could bind and capture MSCs effectively.

NAB Promotes The Reconstruction Of Bone Defects In Vivo

The ethical and legal approval of animal study in this paper was obtained prior to the commencement of the study by the Ethics Committee of Xi'an Children's Hospital, Xi'an, China (no. C2018004). All animal experiments were conducted in accordance with institutional regulations. All experiments were performed following relevant named institutional and national guidelines and regulations. To evaluate whether NAB could enrich MSCs and promote

the reconstruction of bone defects in vivo, an animal model was prepared. Penetrating defects were created in the femurs of rats. NAB (100 mg/kg), random DNA (100 mg/kg) or saline were administrated by iv injections each day, the perforated bones collected were at 2 or 4 weeks. To observe the enrichment of MSCs and bone repair, H&E staining was applied to observe the hematoma reactions of bone marrow, which indicated the early repair process of bone defect. Alizarin red staining was applied for observing the osteoblasts which were differentiated from MSCs. As shown in Figure 7A, at 0 week after bone drilling, a large number of inflammatory cells and red blood cells infiltrated in the bone marrow cavity, and a small amount of scattered bone fragments could be observed; At 2 weeks,

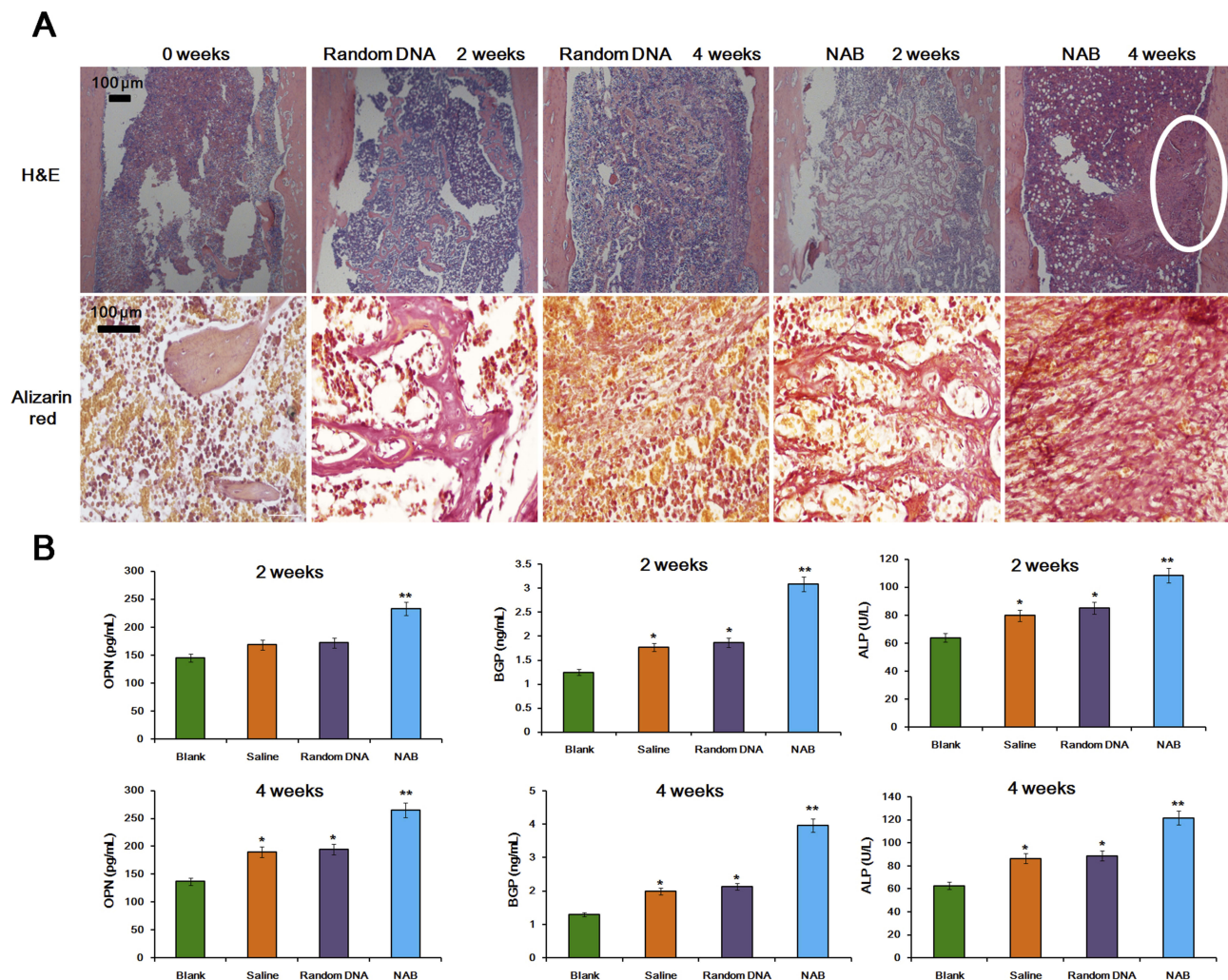


Figure 7 Potential MSCs recruitment by NAB in vivo. **(A)** H&E staining and Alizarin red staining. Representative H&E staining (20 \times) showed that hematomas, accompanied by lots of trabecular bone growth could be observed in the NAB group at 2 weeks, while the random DNA group was not that obvious; At 4 weeks, the trabecular bone growth the NAB group gradually matured. Absorption and shaping occurred. Attaching growth of bone could be observed on the inner side of the cortical bone as the white circle highlighted, while the control group remained in the trabecular bone growth stage. Alizarin red staining (40 \times) images of bone defect region show distinct calcium contents between NAB and random DNA group at either 2 weeks or 4 weeks. **(B)** Serology assessment. Serum markers of osteogenic processes such as OPN, BGP, and ALP were analyzed at the 2 or 4 weeks after the initiation regimen. Each bar represents means with SD of six replicates. * $P < 0.05$; ** $P < 0.01$.

inflammatory cells and red blood cells in the bone marrow cavity were replaced by hematomas, accompanied by lots of trabecular bone growth in the NAB group, while the random DNA group was not that obvious; At 4 weeks, the trabecular bone growth the NAB group gradually matured. In addition, absorption and shaping occurred. Attaching growth of bone could be observed on the inner side of the cortical bone, while the control group remained in the trabecular bone growth stage. Thus, the histomorphological study results indicated that the organized hematoma and cell growth in the bone marrow of the NAB group were more vigorous than that of random library group in both 2 weeks and 4 weeks. Alizarin red staining showed that the red staining of osteoblast cells in the NAB group was significantly denser than that in the random library group in both 2 weeks and 4 weeks, which reflected that NAB has a higher recruitment effect on MSCs. To further evaluate the bone defect reconstruction of NAB, since OPN, BGP, and ALP were secreted by osteoblast and could reflect the generation of osteogenesis, their expression level in rats was analyzed. As presented in Figure 7B, when compared with a blank group (rats without penetrating defects), serum OPN, BGP, and ALP level in saline group, random DNA group, and NAB group at both 2 and 4 weeks were increased, indicating the repair and osteogenesis generation. It is a remarkable fact that OPN, BGP, and ALP concentrations in NAB groups were much higher than that of in saline group and random DNA group ($P < 0.01$), which suggested more osteogenesis generation caused by NAB. To observe the reconstruction of penetrating defects more intuitively, X-ray was applied. As shown in Figure 8, it was found that at 2 weeks, the healing of bone defects in the NAB group were significantly better than the other two groups, the defects became blurred, and local trabecular bone growth could be observed. There was no significant difference between the saline group and the random library group. At 4 weeks, bone defects in the control group and random library group grew to varying degrees, while the NAB group healed satisfactorily, the perforations were barely visible, and the osteotylus growth could be observed outside the cortical bone. These data suggested that NAB could enrich MSCs and improve the repair and restore of bone defect.

Discussion

In this study, using whole-cell SELEX technology, we first developed MSCs aptamer HM69, with Kd of 9.67 nM. It was found that HM69 could recognize and capture MSCs selectively. Further, the first, novel, and effective

nanoparticle termed as NAB based on HM69 was fabricated. We have proven that NAB not only exhibited MSCs recruitment capacity but also achieved a better repair outcome than that of the control group *in vivo*.

Comminuted fracture is a kind of severe fractures in orthopedics.²⁸ In the clinical diagnosis and treatment of trauma orthopedics, strong fixation of fractures and early functional exercise after comminuted fracture are important factors of the rehabilitation of patients.²⁹ Delayed healing of the fracture may cause problems such as muscle atrophy, joint stiffness, and even the nonunion of bone. Whether the anatomical reduction emphasized by AO (Arbeitsgemeinschaft für Osteosynthesefragen), or the functional reduction from the scholars of BO (biological osteosynthesis) or minimally invasive orthopedics, are all for the purpose of early healing and early exercise. When encountering comminuted fractures, delayed healing or non-union became more serious.³⁰ Currently, the methods for early healing have been confirmed by basic experimental studies and clinical studies. For example, the differentiation of mesenchymal stem cells (MSCs) into osteoblasts and chondrocytes for bone repair;^{16,17,28,29} Bone tissue engineering scaffolds, 3D biomanufacturing, bioprinting techniques, and 3D printing, which play a crucial role in repairing bone defects and artificial bone tissue engineering;^{31–33} Non-invasive such as low-intensity pulsed ultrasound (LIPUS) is used to promote healing of bone defects.³⁴ However, these non-invasive treatments are mainly used for the stable, neatly aligned bone defects in adult patients. As for larger bone defects such as comminuted fractures, it is difficult to achieve the desired therapeutic effect.³⁵ The reduction of the comminuted fracture is difficult, and bone defects occur frequently. The comminuted fracture is more likely to damage the surrounding soft tissue and is prone to damage the artery, vein and nerve. Therefore, the probability of nonunion after comminuted fracture is much higher. Clinically, autologous bone grafting is the main method for the repair of comminuted fracture, has become “the gold standard” for the treatment of nonunion of comminuted fracture. However, in recent years, some literature reports have shown that there are some major drawbacks in autologous transplantation, such as pain in the donor region, hematoma in the bone graft area, nerve damage and paresthesia, and even infections. In addition, limited bone mass, prolonged operation time and extra bleeding during surgery add to the disadvantages of autologous bone grafting.^{36,37} Furthermore, the bone graft may also have risks of

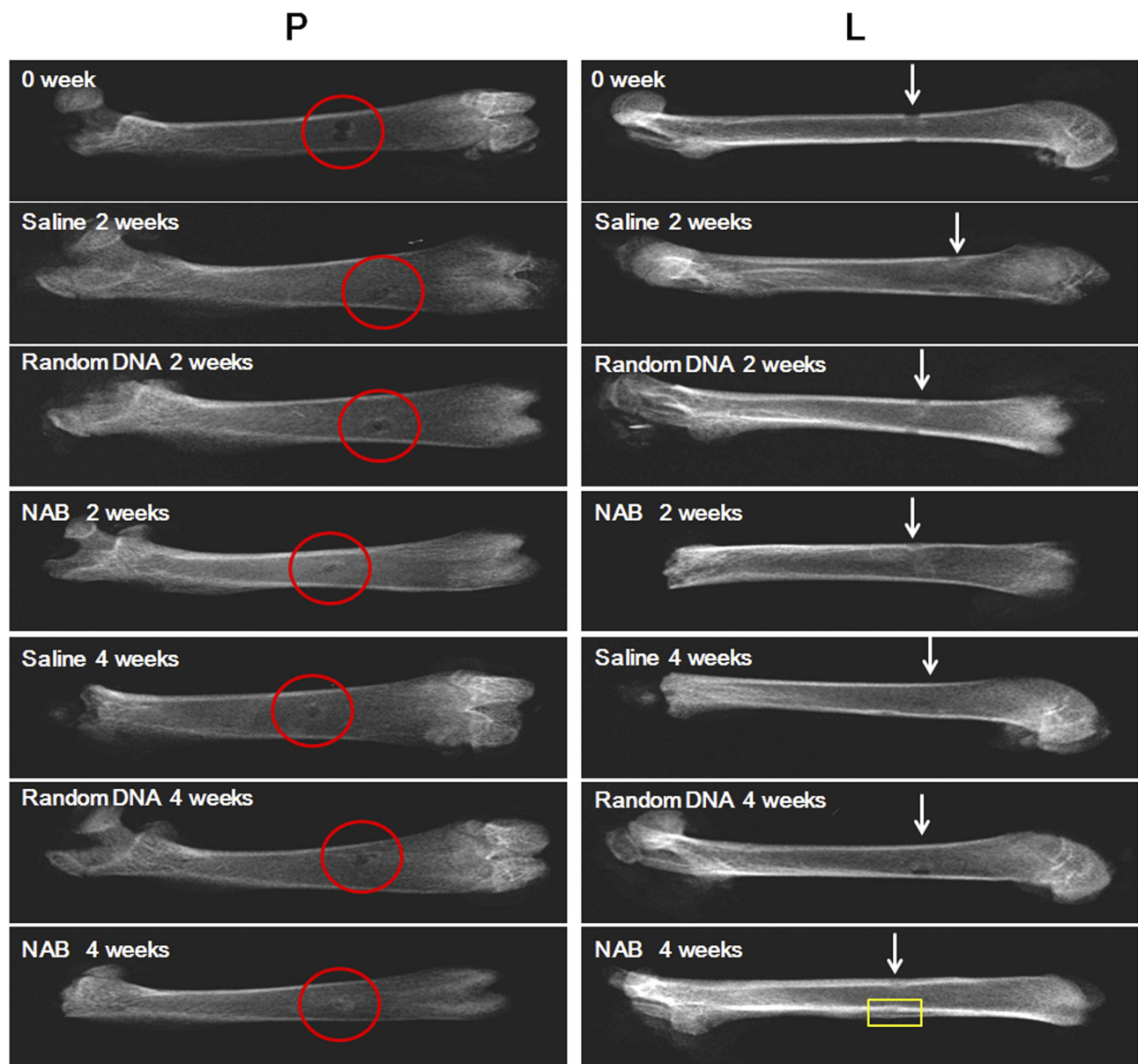


Figure 8 Potential bone defect repair and restoration of NAB in vivo. Penetrating defects were created in the femurs of rats. NAB (100 mg/kg), random DNA (100 mg/kg) or saline were administrated by iv injections each day, the perforated bones collected were at 2 or 4 weeks. X-ray was utilized to observe the reconstruction of penetrating defects. At 2 weeks, the healing of bone defects in the NAB group was blurred as the arrow pointed. At 4 weeks, the NAB group healed satisfactorily, the perforations were barely visible, and the osteotylus growth could be observed outside the cortical bone as the yellow square highlighted (The red circle and white arrow presents the bone defect; The yellow square presents osteotylus growth).

position changing and bone absorbing, sclerosis and necrosis, still resulting in bone defects. Therefore, for comminuted fracture, it is much more difficult to reach early fracture healing, which may delay the functional exercise and worsens the prognosis. Therefore, our research group aims to find a novel way to repair the bone defect caused by comminuted fracture.

Experiments have shown that one of the reasons for the delayed healing or non-union of the fracture is the reduction in the number or the quality of stem cells,³⁸ and MSCs can

promote the repair of segmental bone defects after being implanted in the scaffold material.³⁹ Thus, the targeted enrichment of MSCs to bone defect is a new way to improve the healing of comminuted fracture. At present, some researchers have focused on the device's development of targeted MSCs enrichment. Xin Wang has developed a reinforced sponge/hydrogel scaffold which functionalized with the non-immunogenic aptamer Apt19s to obtain the ability of recruiting endogenous MSCs.⁴⁰ They have demonstrated that this aptamer-functionalized scaffold indeed enhanced endogenous stem cell

homing and promoted cartilage repair as compared with the control group and the scaffold-only group. Xiaoxia Hu also unitized aptamer Apt19s and have designed an aptamer-bilayer scaffold, which was implanted into the osteochondral defect for cartilage regeneration.⁴¹ This aptamer-bilayer scaffold showed excellent performance for osteochondral knee joint and has been demonstrated to be a potential scaffold for knee repair. Thus, aptamer-directed stem cell enrichment is a promising and potential method for tissue-engineering bone repair. All these methods are based on scaffold that implanted into the bone defect. Although these scaffolds showed excellent performance, there are some deficiencies. Firstly, these scaffolds usually need a complex manufacturing process. To achieve the best repair effect, the scaffolds need to mimic the structure of the bone unit for supporting bone generation. This process needs precise design and manufacturing, even needs 3D printing to suit individuals, which may increase the cost. Secondly, to implant scaffold accurately, an effective surgical treatment is necessary. The scaffold should be implanted on fracture reduction seamlessly. However, it cannot be ensured in clinical work due to the different degrees of trauma. Comminuted fracture often accompanied by severe surrounding tissue damage, and even artery, vein and nerve damage, which are difficult to implant such scaffold. Thus, to overcome such a shortage, in this study, we designed novel nanoparticles to restore bone defects that are not independent of scaffold. We generated a novel aptamer termed HM69 which could recognize and bind with MSCs effectively. When compared with the previous aptamer Apt19s,⁴² HM69 exhibited with better binding specificity and affinity. Then, we linked aptamer HM69 with each other to generate novel multi-aptamer nanoparticles which were termed as NAB. When NAB was injected in vivo, it could firstly recognize the MSCs existed in the bone defect and anchored immediately. Then, NAB could capture more MSCs to bone defect to repair. When compared with scaffold, NAB possesses a number of advantages: 1. Non-invasive: NAB could be implanted without surgery, just by injection through veins or directly bones; 2. Higher feasibility: surgical treatment is not necessary for implanting. NBA can function just by injecting; 3. Limited synthesis cost: whether the synthesis of HM69, or the polymerization of HM69 to generate NAB, the cost is much lower than to manufacture scaffold; 4. No batch-to-batch variability. Our data have proved that NAB could enrich MSCs and improve the repair and restore of bone defect. Above all, NAB can be treated as a potential way for bone defect repair and worthy of further investigation toward clinical application. In addition, this aptamer-directed strategy can also serve as an effective approach for cell recruitment in

targeted therapy and is anticipated to find broad application in regenerating new tissues and organs. Our future work will focus on the source of the recruited cell since there is strong evidence for the involvement of synovium derived MSCs in bone repair, and pharmacokinetics of NAB needs further investigation.

Conclusion

In summary, we developed the de novel MSCs aptamer HM69 and generated the first functional nanoparticles termed as NAB based on HM69. Our results demonstrated aptamer HM69 was found capable of recognizing and binding MSCs with high specificity and affinity and obtaining the recruiting endogenous MSCs. Further, the aptamer HM69-functionalized nanoparticles indeed enhanced endogenous stem cell homing and promoted bone defect repair as compared with the control group. Collectively, these features are poised to make MSCs aptamer HM69 uniquely attractive for targeted MSCs enrichment. It is obvious that NAB has great potential application for the development of novel non-invasive bone defect repair and restoration system and may offer a tissue-engineering approach for the treatment of osteochondral lesions.

Funding

This work was funded by Shaanxi key research and development program (2019SF-207& 2017SF-280); Xi'an Science and Technology program SF1510(4).

Disclosure

The authors declare no conflicts of interests in this work.

References

- Downey MW, Lai TC, Fleming JJ. Primary arthrodesis in severely comminuted fractures. *Clin Podiatr Med Surg*. 2018;35(2):233–257. doi:10.1016/j.cpm.2017.12.006
- Ratajczak K, Szczesny G, Malczyk P. Comminuted fractures of the proximal humerus - principles of the diagnosis, treatment and rehabilitation. *Ortop Traumatol Rehabil*. 2019;21(2):77–93. doi:10.5604/01.3001.0013.1544
- Zura R, Braid-Forbes MJ, Jeray K, et al. Bone fracture nonunion rate decreases with increasing age: a prospective inception cohort study. *Bone*. 2017;95:26–32. doi:10.1016/j.bone.2016.11.006
- Ding L, He Z, Xiao H, Chai L, Xue F. Factors affecting the incidence of aseptic nonunion after surgical fixation of humeral diaphyseal fracture. *J Orthop Sci*. 2014;19(6):973–977. doi:10.1007/s00776-014-0640-1
- Fong K, Truong V, Foote CJ, et al. Predictors of nonunion and reoperation in patients with fractures of the tibia: an observational study. *BMC Musculoskelet Disord*. 2013;14:103. doi:10.1186/1471-2474-14-103
- Filipowska J, Tomaszewski KA, Niedźwiedzki Ł, Walocha JA, Niedźwiedzki T. The role of vasculature in bone development, regeneration and proper systemic functioning. *Angiogenesis*. 2017;20(3):291–302. doi:10.1007/s10456-017-9541-1

7. Trickett RW. Letter to the editor Re: the use of dorsal distraction plating for severely comminuted distal radius fractures: a review and comparison to volar plate fixation by R. Perlua, J. Doyona and P. Henryb. *Injury*. 2019. doi:10.1016/j.injury.2019.05.013
8. Perlus R, Doyon J, Henry P. The use of dorsal distraction plating for severely comminuted distal radius fractures: a review and comparison to volar plate fixation. *Injury*. 2019;50(Suppl 1):S50–S55. doi:10.1016/j.injury.2019.03.052
9. Sgromolo NM, Rhee PC. The role of vascularized bone grafting in scaphoid nonunion. *Hand Clin*. 2019;35(3):315–322. doi:10.1016/j.hcl.2019.03.004
10. Mortada I, Mortada R. Epigenetic changes in mesenchymal stem cells differentiation. *Eur J Med Genet*. 2018;61(2):114–118. doi:10.1016/j.ejmg.2017.10.015
11. Huang J, Lu W, Ouyang H, et al. Transplantation of mesenchymal stem cells attenuates pulmonary hypertension by normalizing the EndMT. *Am J Respir Cell Mol Biol*. 2019. doi:10.1165/rcmb.2018-0165OC
12. Scheper V, Schwieger J, Hamm A, Lenarz T, Hoffmann A. BDNF-overexpressing human mesenchymal stem cells mediate increased neuronal protection in vitro. *J Neurosci Res*. 2019;97:1414–1429. doi:10.1002/jnr.v97.11
13. Moshrefi M, Yari N, Nabipour F, Bazrafshani MR, Nematollahi-Mahani SN. Transplantation of differentiated umbilical cord mesenchymal cells under kidney capsule for control of type I diabetes in rat. *Tissue Cell*. 2015;47(4):395–405. doi:10.1016/j.tice.2015.04.008
14. Stiner R, Alexander M, Liu G, et al. Transplantation of stem cells from umbilical cord blood as therapy for type I diabetes. *Cell Tissue Res*. 2019. doi:10.1007/s00441-019-03046-2
15. Zhang B, Zhao N, Zhang J, Liu Y, Zhu D, Kong Y. Mesenchymal stem cells rejuvenate cardiac muscle through regulating macrophage polarization. *Aging (Albany NY)*. 2019;11(12):3900–3908. doi:10.18632/aging.102009
16. Barcak EA, Beebe MJ. Bone morphogenetic protein: is there still a role in orthopedic trauma in 2017? *Orthop Clin North Am*. 2017;48(3):301–309. doi:10.1016/j.jocl.2017.03.004
17. Venkatesan J, Bhatnagar I, Manivasagan P, Kang K-H, Kim S-K. Alginate composites for bone tissue engineering: a review. *Int J Biol Macromol*. 2015;72:269–281. doi:10.1016/j.ijbiomac.2014.07.008
18. Chen W, Sun Y, Gu X, et al. Conditioned medium of mesenchymal stem cells delays osteoarthritis progression in a rat model by protecting subchondral bone, maintaining matrix homeostasis, and enhancing autophagy. *J Tissue Eng Regen Med*. 2019. doi:10.1002/term.v13.9
19. Moccia F, Riccardi C, Musumeci D, et al. Insights into the G-rich VEGF-binding aptamer V7t1: when two G-quadruplexes are better than one! *Nucleic Acids Res*. 2019. doi:10.1093/nar/gkz589
20. Chen K, Fu T, Sun W, et al. DNA-supramolecule conjugates in theranostics. *Theranostics*. 2019;9(11):3262–3279. doi:10.7150/tno.31885
21. Ali MH, Elsherbiny ME, Emara M. Updates on aptamer research. *Int J Mol Sci*. 2019;20:10. doi:10.3390/ijms20102511
22. Esposito CL, Catuogno S, Condorelli G, Ungaro P, de Franciscis V. Aptamer chimeras for therapeutic delivery: the challenging perspectives. *Genes (Basel)*. 2018;9:11. doi:10.3390/genes9110529
23. Bock LC, Griffin LC, Latham JA, Vermaas EH, Toole JJ. Selection of single-stranded DNA molecules that bind and inhibit human thrombin. *Nature*. 1992;355(6360):564–566. doi:10.1038/355564a0
24. Qin Y, Yang X, Zhang J, Cao X. Target capturing performance of microfluidic channel surface immobilized aptamers: the effects of spacer lengths. *Biomed Microdevices*. 2019;21(3):54. doi:10.1007/s10544-019-0403-z
25. Abate MF, Jia S, Ahmed MG, et al. Visual quantitative detection of circulating tumor cells with single-cell sensitivity using a portable microfluidic device. *Small*. 2019;15(14):e1804890. doi:10.1002/sml.v15.14
26. Li F, Hu S, Zhang R, Gu Y, Li Y, Jia Y. Porous graphene oxide enhanced aptamer specific circulating-tumor-cell sensing interface on light addressable potentiometric sensor: clinical application and simulation. *ACS Appl Mater Interfaces*. 2019;11(9):8704–8709. doi:10.1021/acsami.8b21101
27. Wu H, Wang M, Dai B, et al. Novel CD123-aptamer-originated targeted drug trains for selectively delivering cytotoxic agent to tumor cells in acute myeloid leukemia theranostics. *Drug Deliv*. 2017;24(1):1216–1229. doi:10.1080/10717544.2017.1367976
28. Dimitriou R, Tsiridis E, Giannoudis PV. Current concepts of molecular aspects of bone healing. *Injury*. 2005;36(12):1392–1404. doi:10.1016/j.injury.2005.07.019
29. Shrivats AR, McDermott MC, Hollinger JO. Bone tissue engineering: state of the union. *Drug Discov Today*. 2014;19(6):781–786. doi:10.1016/j.drudis.2014.04.010
30. Alierta JA, Pérez MA, Seral B, García-Aznar JM. Biomechanical assessment and clinical analysis of different intramedullary nailing systems for oblique fractures. *Comput Methods Biomech Biomed Engin*. 2016;19(12):1266–1277. doi:10.1080/10255842.2015.1125473
31. Xavier JR, Thakur T, Desai P, et al. Bioactive nanoengineered hydrogels for bone tissue engineering: a growth-factor-free approach. *ACS Nano*. 2015;9(3):3109–3118. doi:10.1021/nn507488s
32. Li C, Gerhart LM, Harrison SP, Ward JK, Harris JM, Prentice IC. RhBMP-2 loaded 3D-printed mesoporous silica/calcium phosphate cement porous scaffolds with enhanced vascularization and osteogenesis properties. *Sci Rep*. 2017;7:41331. doi:10.1038/srep43087
33. Kieser DC, Ailabouni R, Kieser SCJ, et al. The use of an Ossis custom 3D-printed tri-flanged acetabular implant for major bone loss: minimum 2-year follow-up. *Hip Int*. 2018;28(6):668–674. doi:10.1177/1120700018760817
34. Zura R, Mehta S, Rocca GJD et al. A cohort study of 4,190 patients treated with low-intensity pulsed ultrasound (LIPUS): findings in the elderly versus all patients. *BMC Musculoskelet Disord*. 2015;16:45.
35. Higgins A, Glover M, Yang Y, Bayliss S, Meads C, Lord J. EXOGEN ultrasound bone healing system for long bone fractures with non-union or delayed healing: a NICE medical technology guidance. *Appl Health Econ Health Policy*. 2014;12(5):477–484. doi:10.1007/s40258-014-0117-6
36. Slette EL, Mikula JD, Turnbull TL, Hackett TR. Treatment of Midshaft Clavicle fractures: application of local autograft with concurrent plate fixation. *Arthrosc Tech*. 2016;5(3):e557–e562. doi:10.1016/j.eats.2016.02.008
37. Radcliff K, Hwang R, Hilibrand A, et al. The effect of iliac crest autograft on the outcome of fusion in the setting of degenerative spondylolisthesis: a subgroup analysis of the Spine Patient Outcomes Research Trial (SPORT). *J Bone Joint Surg Am*. 2012;94(18):1685–1692. doi:10.2106/JBJS.K.00952
38. Makino T, Hak DJ, Hazelwood SJ, Curtiss S, Reddi AH. Prevention of atrophic nonunion development by recombinant human bone morphogenetic protein-7. *J Orthop Res*. 2005;23(3):632–638. doi:10.1016/j.orthres.2004.09.009
39. Kruyt M, De Bruijn J, Rouwkema J, et al. Analysis of the dynamics of bone formation, effect of cell seeding density, and potential of allogeneic cells in cell-based bone tissue engineering in goats. *Tissue Eng Part A*. 2008;14(6):1081–1088. doi:10.1089/ten.tea.2007.0111
40. Wang X, Song X, Li T et al. Aptamer-functionalized bioscaffold enhances cartilage repair by improving stem cell recruitment in osteochondral defects of rabbit knees. *Am J Sports Med*. 2019;47(10):363546519856355.
41. Hu X, Qu Y, Gupta TD, et al. A difunctional regeneration scaffold for knee repair based on aptamer-directed cell recruitment. *Adv Mater*. 2017;29:15. doi:10.1002/adma.201700681
42. Hou Z, Meyer S, Propson NE, et al. Characterization and target identification of a DNA aptamer that labels pluripotent stem cells. *Cell Res*. 2015;25(3):390–393. doi:10.1038/cr.2015.7

International Journal of Nanomedicine

Dovepress

Publish your work in this journal

The International Journal of Nanomedicine is an international, peer-reviewed journal focusing on the application of nanotechnology in diagnostics, therapeutics, and drug delivery systems throughout the biomedical field. This journal is indexed on PubMed Central, MedLine, CAS, SciSearch[®], Current Contents[®]/Clinical Medicine,

Journal Citation Reports/Science Edition, EMBase, Scopus and the Elsevier Bibliographic databases. The manuscript management system is completely online and includes a very quick and fair peer-review system, which is all easy to use. Visit <http://www.dovepress.com/testimonials.php> to read real quotes from published authors.

Submit your manuscript here: <https://www.dovepress.com/international-journal-of-nanomedicine-journal>